QUANTIFICATION AND VISUALIZATION OF LOCALIZED AND INTUITIVE SHAPE VARIABILITY USING A NOVEL MEDIAL-BASED SHAPE REPRESENTATION

G. Hamarneh, A. D. Ward, R. Frank

Medical Image Analysis Lab, Simon Fraser University, Canada

ABSTRACT

Quantification and visualization of anatomical shape variability in different populations is essential for diagnosis and tracking progression of diseases. We present a new 3D medial-based shape representation method capable of analysis and visualization of 3D anatomy and demonstrate its ability to quantify and highlight shape variability in an intuitive manner. 3D shapes are represented via orientations and elongations of one or more medial sheets, along with thickness values encoding the distances to the shape surface. Two parameters traverse each medial sheet and are mapped to orientation, elongation, and thickness values; we call this map a *medial patch*. Shape variability is decomposed intuitively into bend, stretch, or bulge deformations, via operators acting on the components of the medial patch. In a simple manner, the location, extent, type, and amplitude of the deformation operators can be specified to capture local and global intuitive shape variability. We demonstrate the capabilities and intuitiveness of this approach through synthetic 3D shape deformations, as well as deformations that capture the 3D shape of an anatomical structure. We demonstrate the ability to highlight regions containing specific types of intuitive changes in anatomy.

1. INTRODUCTION

Neurological, cardiological, skeletal, and other pathologies often correlate to shape deviations from the space of normal shapes. Structural abnormality can also indicate increased likelihood of future occurrence of diseases or injuries. Medical imaging is allowing exceptional views of internal anatomy and providing an unprecedented opportunity for disease diagnosis/prediction, prevention, and treatment. Establishing a concise relationship between pathology and 3D anatomical shapes is therefore a desirable goal.

Shape representation is important for segmentation, recognition, and interpretation of medical images [1]. Designing a shape representation that encodes intuitive shape deformations and captures statistical shape variability, for both simple and complex geometry and topology, remains a challenge. Many boundary-based deformable shape representations have been previously proposed, (e.g. SPHARM [2], NURBS [3], superquadrics [4], Wavelet-based [5]). Volume-based shape representations have also been proposed, including those that are based on finite element methods [6]. However, the majority of existing techniques are incapable of decomposing shape variability into intuitive deformations, *easily communicated to clinical experts*, since their deformations are not based on object-relative geometry. Medial axis-based shape representations (MSRs) are emerging as a powerful alternative [7, 8, 9].

In this paper, we present a new MSR-inspired 3D shape representation. It allows for analysis of 3D anatomical shapes, where shape differences are decomposed into independent, intuitive deformation types (bending, stretching, and thickening). We represent the shape of a 3D object as a collection of parts. The different parts are related by an undirected graph encoding the object's topology. To capture the object's geometry, each part is described using a medial sheet with thickness values encoding the distances from the sheets to the object's surfaces. Two parameters traverse each medial sheet and are mapped to the orientation, elongation, and thickness values, which describe the shape of each sheet. Given the analogy of this mapping to a *patch* in differential geometry and the medial-based nature of our shape representation, we refer to our technique as *Medial Patches* (MPs).

In section 2, we describe the shape representation and methods for its computation. Section 3 demonstrates the highlighting of regions having specific types of intuitive changes in anatomy, and in section 4 we give our conclusions.

2. METHOD

2.1. The medial patch shape representation

We represent the shape of a 3D object using a coarse-to-fine approach through a collection of medial sheets, joined via an undirected graph $G(V, E)$ where each vertex V represents a sheet, and each edge E represents a connection between two sheets. Each medial sheet is parameterized on (i, j) [1] where $i, j \in \mathbb{N}$, and comprises a *base medial curve* sampled at *base medial nodes* and several *medial curves* sampled at *medial nodes* and attached to the base medial nodes (figure 1). As-

[1] Without loss of generality, we make the arbitrary choice that nodes where $j = 1$ are base medial nodes. An $O(n)$ operation is required to transform a given shape to place the base medial nodes along $i = 1$ (and vice-versa).

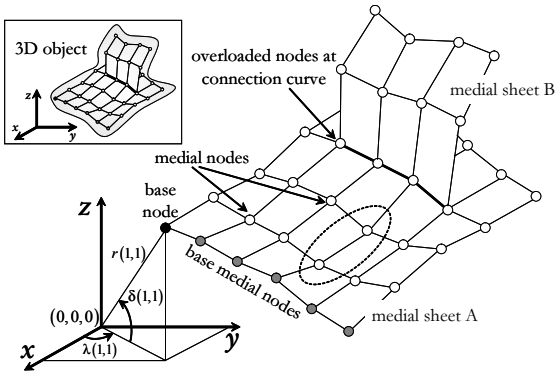

Fig. 1. Terminology and variables of MPs. Elliptic dashed region scaled up in figure 2.

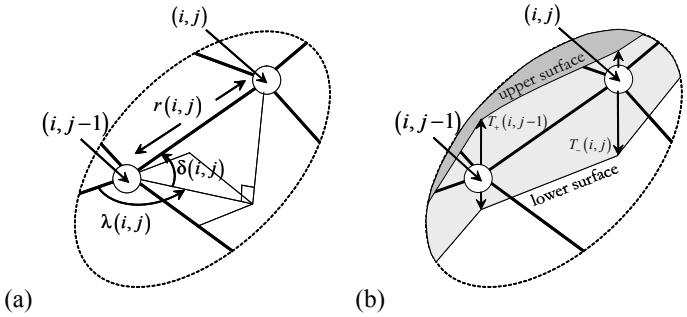

(a) (b)

Fig. 2. Detailed view of (a) longitudinal angle $\lambda(i,j)$, latitudinal angle $\delta(i,j)$ and elongation $r(i,j)$, (b) the distances above $T_+(i,j)$ / below $T_-(i,j)$ the medial sheet.

sociated with each of the medial nodes is a description of the *relative* orientation and spacing between nodes, and thickness values giving two *surface nodes*, which are point samples lying on the object's surface. Medial sheets are joined via *overloaded nodes* which serve as medial nodes for one sheet and as base medial nodes for another (figure 1).

A discrete patch[2] is a map $M : \mathbb{N}^2 \rightarrow \mathbb{R}^n$. We encode each medial sheet using a MP of the form $M : \mathbb{N}^2 \rightarrow \mathbb{R}^5$, with medial sheet parameters (i,j) forming the map's domain. The map's range has five scalar components, three of which encode *relative* positional information about the medial nodes: (1) the elongation (distance), $r(i,j)$, between neighbouring nodes, (2) the longitudinal and (3) latitudinal angles, $\lambda(i,j)$ and $\delta(i,j)$ respectively, between neighbouring nodes (figure 2(a)). Two additional thickness components, $T_+(i,j)$ and $T_-(i,j)$, store the distance above and below the medial sheet[3], respectively, to the upper and lower parts of the surface of the object, defining surface nodes (figure 2(b)).

[2]Based on the definition of a patch in differential geometry; a map $M : \mathbb{R}^2 \rightarrow \mathbb{R}^n$.

[3]$T_+(i,j)$ and $T_-(i,j)$ may be different, per our adoption of a position of practicality over bijection (see section 2.2).

2.2. Computing a medial patch of a 3D object

In this section, we describe and give our rationale for our approach to computing the medial sheet for a given anatomical structure. The decision of how to compute a MSR for a shape depends on one's position on a continuum of bijectivity versus practicality. At one end (bijectivity) sit skeletonization approaches (e.g. [7]), where medial loci are defined as centers of inscribed spheres touching two or more surface points. This yields a bijection between shapes and their MSRs. At the other end (practicality), this bijection does not exist; medial loci may be not truly medial. MSRs that ensure bijectivity are known to be generally very sensitive to small changes at object boundaries. Our representation does not force any position on this continuum. However, in this work we adopt a position of practicality; we encode small, simple protrusions and indentations of objects as changes to thickness values rather than changes to the medial sheet itself. We represent our shape with a sufficiently large number of medial sheets to ensure that these indentations and protrusions can be described by changes in thickness. Specifically, if a protrusion is too complex to be described as an increase in thickness then this warrants a new additional medial sheet to the graph.

The approach used to compute a MP representation of a 3D object is described in algorithm 1, and involves the deformation of an initialized planar sheet according to the shape of the object. Similarly, multiple connected planar sheets can be initialized and deformed to fit to complex objects. The rationale behind this approach is similar to that for the fixed topology skeleton [10]; the topology of the anatomical structure is often known in advance, so spurious skeleton branches can be avoided by fixing the topology of the skeleton.

Algorithm 1 Deforming a flat sheet to a medial sheet of a binary object

Input: Binary volume V; $V(x,y,z) = 1, \forall (x,y,z)$ inside the object
Output: The 3D coordinates $N(i,j)$ of a medial sheet and $N_+(i,j)$, $N_-(i,j)$ of upper and lower implied surfaces of the input object

1: $\lambda_1, \lambda_2, \lambda_3, e_1, e_2, e_3 \leftarrow$ Eigenvectors λ_i and eigenvalues e_i resulting from principal component analysis of $\{x,y,z \mid V(x,y,z) = 1\}$
2: $N(i,j) \leftarrow$ A uniform rectilinear grid of medial nodes lying on a medial sheet with principal directions along λ_1, λ_2, and extents proportional to e_1, e_2
3: **repeat**
4: **for all** nodes (i,j) in the medial sheet **do**
5: $\overrightarrow{Q} \leftarrow$ Normal vector to the medial sheet at (i,j)
6: Cast rays from $N(i,j)$ along $\overrightarrow{Q}$ and $-\overrightarrow{Q}$ until they exit the object. Record the two object exit points as surface nodes $N_+(i,j)$ and $N_-(i,j)$
7: $N(i,j) \leftarrow$ Midpoint of segment from $N_+(i,j)$ to $N_-(i,j)$
8: **end for**
9: **until** no change in $N(i,j), N_+(i,j), N_-(i,j), \forall (i,j)$

Given the 3D coordinates of nodes $N(i,j)$ sampled from (a) medial sheet(s) lying within a 3D object and corresponding surface nodes $N_+(i,j)$ and $N_-(i,j)$ (e.g. from algorithm 1), algorithm 2 computes the object's medial represen-

tation. At each MP domain element (i, j) we compute the patch's range: $r(i, j)$, $\lambda(i, j)$, $\delta(i, j)$, $T_-(i, j)$, and $T_+(i, j)$.

Algorithm 2 Computing a medial patch from medial and surface nodes

Input: The 3D coordinates $N(i, j)$ of a medial sheet and $N_+(i, j)$, $N_-(i, j)$ of upper and lower implied surfaces of the object
Output: A medial patch: $\lambda(i, j), \delta(i, j), r(i, j), T_-(i, j), T_+(i, j)$

for all nodes (i, j) in the medial sheet **do**
  $\Phi(i, j) \leftarrow$ Local coordinate system computed using algorithm 3
  $(x_1, x_2, x_3) \leftarrow$ 3D coordinates $N(i, j)$ transformed from global coordinate system Φ_G to $\Phi(i, j)$
  $r(i, j) \leftarrow \sqrt{(x_1^2 + x_2^2 + x_3^2)}$
  $\lambda(i, j) \leftarrow \tan^{-1}(\frac{x_1}{-x_2})$
  $\delta(i, j) \leftarrow \cos^{-1}(\frac{x_3}{r(i,j)})$
  $T_+(i, j) \leftarrow \|N(i, j) - N_+(i, j)\|$
  $T_-(i, j) \leftarrow \|N(i, j) - N_-(i, j)\|$
end for

We use algorithm 3 to construct[4] a local Cartesian coordinate system $\Phi(i, j)$ with origin $N(i, j)$ and orthonormal basis $\overrightarrow{x_1}$, $\overrightarrow{x_2}$, and $\overrightarrow{x_3}$ at each node (i, j). Using coordinate system $\Phi(i, j)$, the spherical coordinates $r(i, j)$, $\lambda(i, j)$, and $\delta(i, j)$ define $N(i, j)$, as in figure 2(a). The model's pose (figure 1) is controlled by values $\lambda(1, 1)$, $\delta(1, 1)$ and $r(1, 1)$.

Algorithm 3 Computing a local Cartesian coordinate system at a medial node

Input: Parameters (i, j), medial nodes $N(m, n), \forall m = 1..i, n = 1..j$
Output: The orthonormal Cartesian coordinate system $\Phi(i, j)$

if $i = 1$ and $j = 1$ **then** {Base node}
  $\Phi(i, j) \leftarrow$ Global coordinate system Φ_G; Stop
else if $i > 1$ and $j = 1$ **then** {Base medial nodes}
  $(i, j) \leftarrow (i - 1, j)$
else {Medial nodes}
  $(i, j) \leftarrow (i, j - 1)$
end if
if $i = 1$ **then**
  $N(i - 1, j) \leftarrow (1, 0, 0)$
end if
if $j = 1$ **then**
  $N(i, j - 1) \leftarrow (0, 1, 0)$
end if
$\overrightarrow{x_1} \leftarrow \overrightarrow{(N(i, j) - N(i - 1, j))}$
$\overrightarrow{x_2} \leftarrow \overrightarrow{(N(i, j) - N(i, j - 1))}$
$\overrightarrow{\widehat{x}_{2_{\perp x_1}}} \leftarrow \overrightarrow{\widehat{x}_2} - (\overrightarrow{x_1}\overrightarrow{x_1}^T / \overrightarrow{x_1}^T\overrightarrow{x_1})\overrightarrow{\widehat{x}_2}$
{$\overrightarrow{\widehat{x}_{2_{\perp x_1}}}$ is $\overrightarrow{\widehat{x}_2}$'s normal component to $\overrightarrow{x_1}$, in the plane formed by $\overrightarrow{x_1}$ and $\overrightarrow{\widehat{x}_2}$}
$\overrightarrow{x_2} \leftarrow \overrightarrow{\widehat{x}_{2_{\perp x_1}}} / \|\overrightarrow{\widehat{x}_{2_{\perp x_1}}}\|$ {Unit vector}
$\overrightarrow{x_1} \leftarrow \overrightarrow{x_1} / \|\overrightarrow{x_1}\|$ {Unit vector}
$\overrightarrow{x_3} \leftarrow \overrightarrow{x_1} \times \overrightarrow{x_2}$
{$\overrightarrow{x_3}$ is the unit vector normal to $\overrightarrow{x_1}$ and $\overrightarrow{x_2}$ ensuring a right-handed coordinate system}
$\Phi(i, j) \leftarrow$ Origin $N(i, j)$, orthonormal basis vectors $\overrightarrow{x_1}, \overrightarrow{x_2}, \overrightarrow{x_3}$

[4]In algorithm 3, we make an arbitrary yet consistent choice of basis, without loss of generality: for nodes where $i = 1$ or $j = 1$, we are faced with the problem of how to define the local frame of reference at $N(i, j)$ since $N(0, j)$ or $N(i, 0)$ are nonexistent. We replace $N(0, j)$ with $(1, 0, 0)$ and $N(i, 0)$ with $(0, 1, 0)$.

2.3. Shape reconstruction from medial patches

Given a MP, we perform two reconstructions, each mapping $\mathbb{N}^2 \rightarrow \mathbb{R}^3$. The first maps each (i, j) to 3D coordinates of a medial node. The second maps each (i, j) to the 3D coordinates of the object surface above (N_+) and below (N_-) the sheet. The reconstruction process is given in algorithm 4.

Algorithm 4 Shape reconstruction from medial patches

Input: A medial patch: $\lambda(i, j), \delta(i, j), r(i, j), T_-(i, j), T_+(i, j)$
Output: The 3D coordinates $N(i, j)$ of the medial sheet and $N_+(i, j)$, $N_-(i, j)$ of upper and lower implied surfaces of the object

for all nodes (i, j) in the medial sheet **do**
  $\Phi(i, j) \leftarrow$ Local coordinate system computed using algorithm 3
  $x_1 \leftarrow r(i, j) \sin(\lambda(i, j)) \sin(90° - \delta(i, j))$
  $x_2 \leftarrow -(r(i, j) \cos(\lambda(i, j)) \sin(90° - \delta(i, j)))$
  $x_3 \leftarrow r(i, j) \cos(90° - \delta(i, j))$
  $N(i, j) \leftarrow$ 3D coordinates (x_1, x_2, x_3) transformed from $\Phi(i, j)$ to global coordinate system Φ_G
end for
for all nodes (i, j) in the medial sheet **do**
  $\overrightarrow{Q} \leftarrow$ Normal vector to the medial sheet at (i, j)
  $N_+(i, j) \leftarrow T_+(i, j)\overrightarrow{Q}$
  $N_-(i, j) \leftarrow -T_-(i, j)\overrightarrow{Q}$
end for

3. RESULTS

Figure 3 uses deformed synthetic slabs to illustrate the ability of this shape representation to decompose shape variations into intuitive components. Figure 4 illustrates the bending of a single caudate nucleus, as well as the ability to highlight intuitive deformations in local regions.

4. CONCLUSION

We presented a novel 3D shape representation based on medial patches, which represent 3D objects as collections of maps from $\mathbb{N}^2$ to $\mathbb{R}^5$. MPs capture intuitive aspects of individual shapes, and differences between shapes, such as bending, elongation, and thickness, enabling useful visualizations and quantifications, with different potential applications, e.g. highlighting colon polyps. Bending and thickness values from the patches also enable the straightforward calculation of more traditional shape measures such as surface roughness, and curvature. Future work includes providing a means for shape correspondence establishment in the domains of the MPs, enabling deformation, location, and scale-specific statistical analysis of a set of shapes, as done previously in 2D [8]. Future work also includes automatic fitting of MP representations to non-binary data (segmentation), to be achieved by extending our automatic sheet-fitting approach using energy minimization and complex features rather than transitions of binary intensities, as with Deformable Organisms [11].

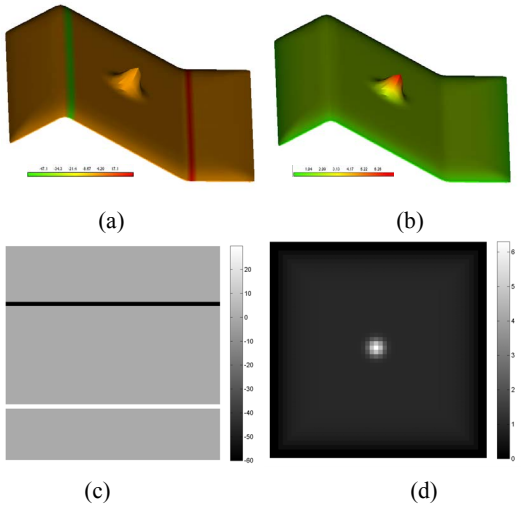

Fig. 3. (a) A bent slab with a protrusion, with only the bending component $\delta(i,i)$ highlighted. (b) Same as (a), with thickness components $(T_+(i,j) + T_-(i,j))$ highlighted. (c),(d) MP range components of bending and thickness, corresponding to (a) and (b), rendered as grayscale images.

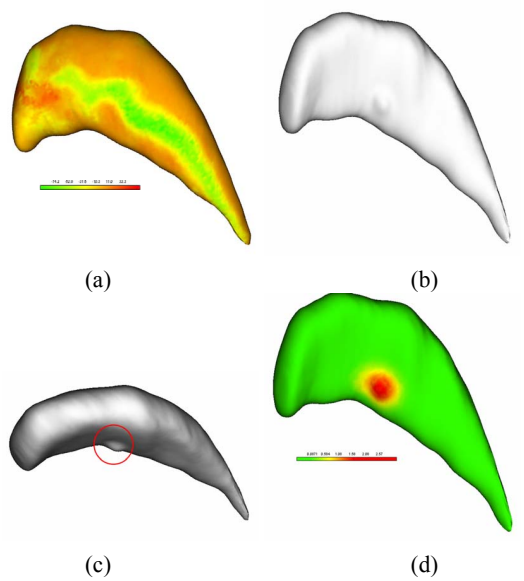

Fig. 4. (a) A caudate nucleus, with warmer colours indicating more bending. (b) A second caudate nucleus, with a small (artificial) protrusion. Note that the protrusion is difficult to see in this view. (c) If the user rotates the view to the correct angle, it may be possible to see this protrusion. (d) The protrusion is captured by our shape representation as a thickness difference as compared with (a), and readily highlighted.

5. ACKNOWLEDGEMENTS

The medical data presented in this paper were provided by Dr. Martin J. McKeown of the Pacific Parkinson's Research Centre, Department of Medicine, University of British Columbia.

6. REFERENCES

[1] I. Dryden and K. Mardia, *Statistical Shape Analysis*, John Wiley and Sons, 1998.

[2] G. Gerig, M. Styner, M. E. Shenton, and J. A. Lieberman, "Shape versus size: Improved understanding of the morphology of brain structures," *Proc. MMBIA 2001, IEEE Computer Society*, pp. 171–178, Dec 2001.

[3] M. Mortenson, *Geometric Modeling*, Wiley, 1997.

[4] D. Terzopoulos and D. Metaxas, "Dynamic 3D models with local and global deformations: deformable superquadrics," *IEEE PAMI*, vol. 13, no. 7, pp. 703–714, 1991.

[5] C. Davatzikos, X. Tao, and D. Shen, "Hierarchical active shape models: Using the wavelet transform," *IEEE Trans. Med. Imag.*, vol. 22, no. 3, pp. 414–423, 2003.

[6] C. Mandal, B. C. Vemuri, and H. Qin, "A new dynamic FEM-based subdivision surface model for shape recovery and tracking in medical images," *MICCAI*, pp. 753–760, 1998.

[7] H. Blum, "Biological shape and visual science," *Theor. Biology*, vol. 38, pp. 205–287, 1973.

[8] G. Hamarneh, R. Abugharbieh, and T. McInerney, "Medial profiles for modeling deformation and statistical analysis of shape and their use in medical image segmentation," *IJSM*, vol. 10, no. 2, pp. 187–209, 2004.

[9] S. Pizer, G. Gerig, S. Joshi, and S. R. Aylward, "Multiscale medial shape-based analysis of image objects," *Proc. IEEE*, vol. 91, no. 10, pp. 1670–1679, 2003.

[10] P. Golland and W. E. L. Grimson, "Fixed topology skeletons," *CVPR*, vol. 1, no. 1, pp. 10–17, 2000.

[11] G. Hamarneh, T. McInerney, and D. Terzopoulos, "Deformable organisms for automatic medical image analysis," *MICCAI*, vol. 2208, 2001.